Advances in Mathematical
Sciences and Applications
Vol. 28, No. 1 (2019), pp. 155–169

GAKKOTOSHO
TOKYO JAPAN

A FIRST-ORDER BI-PROJECTION SCHEME FOR INCOMPRESSIBLE TWO-PHASE BINGHAM FLOWS

Rénald Chalayer

Laboratoire de Mathématiques Blaise Pascal, UMR 6620,
Université Clermont Auvergne and CNRS, Campus des Cézeaux,
3 place Vasarely, TSA 60026 CS 60026, 63178 Aubière cedex, France
(E-mail: Renald.Chalayer@uca.fr)

and

Thierry Dubois

Laboratoire de Mathématiques Blaise Pascal, UMR 6620,
Université Clermont Auvergne and CNRS, Campus des Cézeaux,
3 place Vasarely, TSA 60026 CS 60026, 63178 Aubière cedex, France
(E-mail: Thierry.Dubois@uca.fr)

Abstract. A first-order bi-projection scheme for the numerical simulation of two-phase immiscible, incompressible and isothermal flows of viscoplastic media is presented. As in the Uzawa-like algorithm, the definition of the stress tensor is rewritten in terms of a pointwise projection. A pseudo-time relaxation term is added in order to obtain a geometric convergence of the fixed-point iterations used for the computation of the plastic part of the stress tensor. The coupling between pressure and velocity field is treated with a fractional time-stepping scheme. The interface between the two phases is handled with a level set formulation. Numerical simulations of Rayleigh-Taylor instabilities are performed and presented. The first order rate of convergence with respect to the time step is recovered both in the case of Newtonian and Bingham flows. Comparisons with published results in the case of Newtonian flows validate the parallel implementation of the bi-projection scheme.

Communicated by Messoud Efendiyev; Received February 11, 2019.
AMS Subject Classification: 76T99, 76D05, 76A05, 65M12.
Keywords: Viscoplastic medium, Incompressible two-phase flows, Bingham flows, Projection method, Rayleigh-Taylor instabilities

1 Introduction

Mixture of fluids with different rheology and different physical parameters commonly occurs in geophysical phenomena and environmental problems. For instance, pyroclastic flows are mixtures of granular matter and gas generated by volcanic eruptions in the case of plume or dome collapses. They are a major source of volcanic hazards responsible of considerable damages, injuries and even deaths of human beings in populations leaving nearby volcanos. Pyroclastic flows may sweep along volcano's hills over long distances resulting in areas of several square kilometers covered by a deep layer of granular materials as in the partial dome collapse of Soufrière Hills Volcano in 1997 (see [16]). Another possible scenario is the entrance of a pyroclastic flow into water generating a tsunami which can also be responsible of disasters and may have a deathly impact (see [29, 21]).

The rheology of granular flows is not well understood. Nevertheless, granular flows share characteristic behaviours with flows of viscoplastic medium. Viscoplastic fluids flow ony if the stress exceeds a thresholds otherwise they do not deform and behave like solids. Granular material flows like a fluid over long runout distance but, unlike fluids, they stop in finite time. A model with a rheology similar to the Bingham rheology but with a yield stress depending on the pressure has been applied to the numerical study of the collapse of granular columns (see [14]). The aim of this paper is to propose a new time discretization scheme on a simpler model retaining the complexity of the mixture of two fluids of viscoplastic medium with different physical parameters, namely density, viscosity and yield stress.

In the Bingham rheology, the stress tensor becomes proportional to the strain rate if its strength exceeds the yield stress otherwise it is not prescribed. This model reproduces the peculiar behavior of viscoplastic medium which behaves as a solid when the stress is below the yield stress and flows like a fluid otherwise. The main difficulty both for theoretical and numerical studies of viscoplastic flows relies on the non-differentiable definition of the rheology. From a numerical point of view, the most appealing method due to its simplicity is the regularization method: a *small* parameter is introduced so that the stress tensor becomes everywhere proportional to the strain rate with a spatially variable viscosity which remains finite (see [3, 20] for instance). Regularization methods encounter difficulties in accurately computing the rigid zones separating yielded and unyielded regions (see [8] for detailed study and analysis). The other classical approach relies on the variational formulation of the Navier-Stokes equations leading to an optimization (saddle-point) problem which can be solved with Uzawa-like or augmented Lagrangian algorithms (see [23] for a review). Both methods accurately compute contours of the plug regions but they are quite expansive in terms of number of iterations required to achieve convergence. In the implementation of the Uzawa-like algorithm, the plastic tensor is computed with a pointwise projection operator. A possible way to increase the convergence rate of Picard's iterations used to solve the fixed-point problem coupling the plastic tensor and the velocity field is to introduce a pseudo-time relaxation term. This has been investigated in [6] in the context of projection schemes for the time semi-discretization of the Navier-Stokes equations (see [12]) for incompressible and isothermal Bingham flows in the case of homogeneous flows, *i.e.* with constant density, and recently extended in [4] to the case of flows with spatially variable physical parameters, namely density, viscosity and yield

stress. In [4], a bi-projection scheme has been proposed and analyzed. More precisely, it has been proven to be stable and first-order accurate if the relaxation parameter is properly chosen, *i.e.* if it equals the time step.

The purpose of the paper is to implement the bi-projection scheme analyzed in [4] in the context of the numerical study of two-phase immiscible, icompressible and isothermal flows of viscoplastic medium. A level set formulation is used to track the interface of the fluids. In this approach (see [26, 25]), the interface is the set of points where the level set function vanishes and the latter is transported by the velocity field satisfying the Navier-Stokes equations over the whole domain. For obvious reasons, it is desirable to transport a smooth function rather than a discontinuous one. The level set function is therefore initialized and maintained, with the help of a redistancing procedure, as the normal signed distance function from the interface (see [19]). The reinitialization step consists in solving a Hamilton-Jacobi equation with an artificial time: the stationary solution of which being a distance function (see [25, 22]). It has been observed in [22] that, during iterations of the reinitialization procedure the zeros off the level set function have the tendency to move towards the closest grid point and a subcell fix method has been proposed to remedy this numerical artifact. In [17], the effect of the temporal discretization of the Hamilton-Jacobi coupled with the subcell fix algorithm was studied. These methods have been implemented in the present study.

The paper is organized as follows. In the next section, the mathematical model for the numerical study of two-phase immiscible, icompressible and isothermal flows of viscoplastic medium is introduced. As in [6], the non-differentiable definition of the plastic part of the stress tensor is reformulated with a pointwise projection operator. A non-dimensional form of the equations is proposed. In Section 3, the bi-projection scheme derived from the first-order scheme recently introduced and analyzed in [4] is described. The convergence rate of the fixed-point procedure used to solve the coupling between the velocity field and the plastic tensor is recalled. In Section 4, some details on numerical implementation and spatial discretization are given. Finally, in Section 5, numerical results aiming to assess the accuracy and efficiency of the bi-projection scheme are presented and discussed. The rate of convergence of the time scheme is shown to be first-order for the velocity, the density and the pressure. Numerical experiments of a Rayleigh-Taylor instability finally demonstrate the performance of the bi-projection scheme.

2 A mathematical model for two-phase incompressible Bingham flows

2.1 The level set formulation

In a domain $\Omega \in \mathbb{R}^2$, we consider two immiscible, incompressible and isothermal flows of viscoplastic media separated by an interface $\Gamma(t)$ moving with time $t > 0$. The physical parameters of each phase, *i.e.* the density, viscosity and yield stress, are respectively denoted by ρ_i, μ_i and α_i for $i = 1, 2$. We assume that $\rho_2 \geq \rho_1$. The level set formulation (see [26, 5, 25]) aims to write a system of equations governing both phases and satisfied on

the whole domain Ω by *one* set of global unknowns, namely the velocity field $\mathbf{u}(\mathbf{x},t)$, the pressure $p(\mathbf{x},t)$ and the density $\rho(\mathbf{x},t)$. In this framework, the interface $\Gamma(t)$ corresponds to the set of points where the level set function ϕ vanishes, *i.e.* $\Gamma(t) = \{\mathbf{x} \in \Omega;\ \phi(\mathbf{x},t) = 0\}$. The level set function is a smooth function of $\mathbf{x}$ transported by the flow field. The signed distance function from the interface is commonly used (see [18] and the reference therein). In this context, the level set formulation for two immiscible, incompressible and isothermal flows of viscoplastic media writes

$$\frac{\partial \phi}{\partial t} + \operatorname{div}(\mathbf{u}\phi) = 0 \quad \text{in } \Omega, \tag{1}$$

$$\rho(\phi)\left(\frac{\partial \mathbf{u}}{\partial t} + \operatorname{div}(\mathbf{u}\otimes\mathbf{u})\right) + \boldsymbol{\nabla} p = -\rho(\phi) g \mathbf{e_2} + \operatorname{div}\boldsymbol{\tau}(\phi) \quad \text{in } \Omega, \tag{2}$$

$$\operatorname{div}\mathbf{u} = 0 \quad \text{in } \Omega, \tag{3}$$

where g is the gravitational constant and $\mathbf{e_2} = (0,1)$. Equations (1)-(3) are supplemented by initial and boundary conditions. Note that the surface tension forces are not taken into account. For Bingham type flows, the deviatoric stress tensor is related to the strain rate tensor $\boldsymbol{Du} = \frac{1}{2}\left(\boldsymbol{\nabla u} + {}^t\boldsymbol{\nabla u}\right)$ by

$$\boldsymbol{\tau}(\phi) = 2\mu(\phi)\boldsymbol{Du} + \alpha(\phi)\boldsymbol{\Sigma}$$

with

$$\begin{cases} \boldsymbol{\Sigma} = \frac{\boldsymbol{Du}}{\|\boldsymbol{Du}\|} & \text{if} \quad \boldsymbol{Du} \neq 0, \\ \boldsymbol{\Sigma} \in \Lambda & \text{if} \quad \boldsymbol{Du} = 0, \end{cases} \tag{4}$$

where $\Lambda \equiv \{\boldsymbol{\lambda} \in \mathbb{R}^{2\times 2};\ \|\boldsymbol{\lambda}\| \leq 1 \ a.e. \text{ in } \Omega,\ \operatorname{tr}(\boldsymbol{\lambda}) = 0,\ {}^t\boldsymbol{\lambda} = \boldsymbol{\lambda}\}$ and, for any tensor $\boldsymbol{\lambda} \in \mathbb{R}^{2\times 2}$, $\|\boldsymbol{\lambda}\| = \left(\frac{1}{2}\sum_{i,j}\lambda_{ij}^2\right)^{\frac{1}{2}}$ is its Froebenius norm.

The physical parameters being constant in each phase, we define

$$\rho(\phi) = \rho_1 H(\phi) + \rho_2(1 - H(\phi)), \tag{5}$$

where $H(\phi)$ is the Heaviside function given by

$$H(\phi) = \begin{cases} 1 & \text{if } \phi < 0, \\ \frac{1}{2} & \text{if } \phi = 0, \\ 0 & \text{if } \phi > 0, \end{cases}$$

and similarly for the viscosity $\mu(\phi)$ and the yield stress $\alpha(\phi)$.

2.2 The projection formulation for the Bingham rheology

We now introduce a projection formulation for the plastic part $\boldsymbol{\Sigma}$ of the stress tensor which will be used for the construction of the time discretization. For this purpose, let us introduce the projection operator $\mathbb{P}_\Lambda : \mathbb{R}^{2\times 2} \longrightarrow \Lambda$. If $\boldsymbol{\lambda} \in \mathbb{R}^{2\times 2}$ is a symmetric traceless tensor, then its projection onto Λ is explicit. Indeed, we have, *a.e.* in Ω,

$$\mathbb{P}_\Lambda(\boldsymbol{\lambda}) = \begin{cases} \boldsymbol{\lambda} & \text{if } \|\boldsymbol{\lambda}\| \leq 1, \\ \boldsymbol{\lambda}/\|\boldsymbol{\lambda}\| & \text{if } \|\boldsymbol{\lambda}\| > 1. \end{cases}$$

Note that if $\boldsymbol{\lambda} \in \mathbb{R}^{2\times 2}$ is not traceless then we have $\mathbb{P}_\Lambda(\boldsymbol{\lambda}) = \mathbb{P}_\Lambda\big(\boldsymbol{\lambda} - \frac{1}{2}\mathrm{tr}(\boldsymbol{\lambda})\mathrm{Id}\big)$. With the help of these definitions, it can be easily shown (see [6, 4]) that the following result holds.

Proposition 1 For any positive number ℓ, definition (4) is equivalent to the relation

$$\boldsymbol{\Sigma} \,=\, \mathbb{P}_\Lambda\big(\boldsymbol{\Sigma} + \ell \boldsymbol{D}\boldsymbol{u}\big).$$

With the help of Proposition 1, the mathematical model (1)-(4) can be rewritten as

$$\frac{\partial \phi}{\partial t} + \mathrm{div}(\boldsymbol{u}\phi) = 0, \tag{6}$$

$$\rho(\phi)\left(\frac{\partial \boldsymbol{u}}{\partial t} + \mathrm{div}(\boldsymbol{u}\otimes\boldsymbol{u})\right) - \mathrm{div}(2\mu(\phi)\boldsymbol{D}\boldsymbol{u}) + \boldsymbol{\nabla} p = -\rho(\phi) g \mathbf{e_2} + \mathrm{div}(\alpha(\phi)\boldsymbol{\Sigma}), \tag{7}$$

$$\boldsymbol{\Sigma} \,=\, \mathbb{P}_\Lambda\big(\boldsymbol{\Sigma} + \ell \boldsymbol{D}\boldsymbol{u}\big),\ \ell > 0, \tag{8}$$

$$\mathrm{div}\,\boldsymbol{u} = 0. \tag{9}$$

2.3 A non-dimensional form of the mathematical model

In order to write the system (6)-(9) in dimensionless form, we introduce a characteristic length L and we use the physical parameters of the heavier fluid as reference quantities, namely ρ_2, μ_2 and α_2. As reference velocity $\sqrt{gL}$ is used so that the corresponding reference time is $\sqrt{\frac{L}{g}}$ and the reference pressure is $\rho_2 g L$. By scaling all variables with respect to these reference quantities, the mathematical model in dimensionless form reads

$$\frac{\partial \phi}{\partial t} + \mathrm{div}(\boldsymbol{u}\phi) = 0, \tag{10}$$

$$\rho(\phi)\left(\frac{\partial \boldsymbol{u}}{\partial t} + \mathrm{div}(\boldsymbol{u}\otimes\boldsymbol{u})\right) - \mathrm{div}\big(\frac{2\mu(\phi)}{\mathfrak{Re}}\boldsymbol{D}\boldsymbol{u}\big) + \boldsymbol{\nabla} p = -\rho(\phi)\mathbf{e_2} + \frac{\mathfrak{Bi}}{\mathfrak{Re}}\,\mathrm{div}(\alpha(\phi)\boldsymbol{\Sigma}), \tag{11}$$

$$\boldsymbol{\Sigma} \,=\, \mathbb{P}_\Lambda\big(\boldsymbol{\Sigma} + \ell \boldsymbol{D}\boldsymbol{u}\big),\ \ell > 0, \tag{12}$$

$$\mathrm{div}\,\boldsymbol{u} = 0, \tag{13}$$

where the dimensionless Reynolds and Bingham numbers are respectively defined as

$$\mathfrak{Re} = \frac{\rho_2\sqrt{gL^3}}{\mu_2} \quad \text{and} \quad \mathfrak{Bi} = \frac{\alpha_2\sqrt{L}}{\mu_2\sqrt{g}}.$$

The dimensionless density is derived from (5), that is

$$\rho(\phi) = \frac{\rho_1}{\rho_2}H(\phi) + (1 - H(\phi)), \tag{14}$$

and similarly for the viscosity and the yield stress.

3 The first-order bi-projection scheme

Let $\delta t > 0$ a time step. We define a discrete time sequence $\{t_n; n \geq 0\}$ by $t_n = n\delta t$. The time semi-discretization of Equations (10)-(13) presented hereafter defines sequences $\{\phi^n, \mathbf{u}^n, \mathbf{u}^n_{\rm div}, p^n, \boldsymbol{\Sigma}^n;\, n > 0\}$ which are approximation of the time continuous solutions, *i.e.* $\phi^n \approx \phi(t_n)$. Both $\mathbf{u}^n$ and $\mathbf{u}^n_{\rm div}$ are approximations of the velocity field $\mathbf{u}(t_n)$. However, $\mathbf{u}^n_{\rm div}$ is a divergence-free velocity field while $\mathbf{u}^n$ is not. These sequences are initialized : ρ^0 and $\mathbf{u}^0$ are given, $\boldsymbol{\Sigma}^0 = 0$, $\mathbf{u}^0_{\rm div}$ and p^0 are computed from $\mathbf{u}^0$ so that $\mathrm{div}(\mathbf{u}^0_{\rm div}) = 0$, we finally set $p^{-1} = p^0$.

Let us assume that $(\phi^n, \mathbf{u}^n, \mathbf{u}^n_{\rm div}, p^n, \boldsymbol{\Sigma}^n)$ are known. The first-order bi-projection scheme discretizing (10)-(13) is a fractional time-stepping method derived from [4] and inspired from [10, 11]. It consists in the following successive steps.

1. The discrete level set function ϕ^{n+1} is computed from the transport equation (10) discretized with an explicit RK3 TVD time scheme [24, 9] using $\mathbf{u}^n_{\rm div}$ as transport velocity, *i.e.* we solve the following equations

$$\begin{cases} \frac{\phi^{n,1}-\phi^n}{\delta t} + \mathrm{div}\big(\mathbf{u}^n_{\rm div}\phi^n\big) = 0, \\ \phi^{n,2} = \frac{3}{4}\phi^n + \frac{1}{4}\phi^{n,1} - \frac{\delta t}{4}\,\mathrm{div}\big(\mathbf{u}^n_{\rm div}\phi^{n,1}\big), \\ \frac{\phi^{n,3}-\phi^{n,2}}{\delta t} + \mathrm{div}\big(\mathbf{u}^n_{\rm div}\phi^{n,2}\big) = 0, \\ \phi^{n+1} = \frac{1}{3}\phi^n + \frac{2}{3}\phi^{n,3}. \end{cases} \tag{15}$$

2. The physical parameters are computed from ϕ^{n+1} using (14), that is we set

$$\rho^{n+1} = \rho(\phi^{n+1}),\ \mu^{n+1} = \mu(\phi^{n+1}),\ \alpha^{n+1} = \alpha(\phi^{n+1}).$$

3. Let $\theta \in [0, 1)$ a given *numerical* parameter. The velocity field $\mathbf{u}^{n+1}$ and the plastic tensor $\boldsymbol{\Sigma}^{n+1}$ are solutions of

$$\begin{cases} \rho^{n+1}\Big(\frac{\mathbf{u}^{n+1}-\mathbf{u}^n}{\delta t}\Big) - \mathrm{div}\Big(\frac{2\mu^{n+1}}{\mathfrak{Re}}\boldsymbol{D}\boldsymbol{u}^{n+1}\Big) + \rho^{n+1}\,\mathrm{div}(\mathbf{u}^n_{\rm div}\otimes\mathbf{u}^n) \\ \qquad\qquad +\boldsymbol{\nabla}(2p^n - p^{n-1}) \;=\; -\rho^{n+1}\mathbf{e_2} + \frac{\mathfrak{Bi}}{\mathfrak{Re}}\,\mathrm{div}(\alpha^{n+1}\boldsymbol{\Sigma}^{n+1}), \\ \boldsymbol{\Sigma}^{n+1} = \mathbb{P}_\Lambda\big(\boldsymbol{\Sigma}^{n+1} + \ell\alpha^{n+1}\boldsymbol{D}\boldsymbol{u}^{n+1} + \theta(\boldsymbol{\Sigma}^n - \boldsymbol{\Sigma}^{n+1})\big). \end{cases} \tag{16}$$

4. The pressure increment $p^{n+1} - p^n$ is solution of the Poisson equation

$$\begin{cases} \Delta(p^{n+1} - p^n) = \dfrac{\rho_1}{\delta t}\,\mathrm{div}(\mathbf{u}^{n+1}), \\ \partial_{\boldsymbol{n}}(p^{n+1} - p^n)|_{\partial\Omega} = 0. \end{cases} \tag{17}$$

5. The divergence-free velocity field $\mathbf{u}^{n+1}_{\rm div}$ is obtained by stating

$$\mathbf{u}^{n+1}_{\rm div} = \mathbf{u}^{n+1} - \frac{\delta t}{\rho_1}\boldsymbol{\nabla}(p^{n+1} - p^n). \tag{18}$$

The fact that $\mathrm{div}\,\mathbf{u}^{n+1}_{\rm div} = 0$ is a direct consequence of (17) and (18).

In order to implement the computation of $(\mathbf{u}^{n+1}, \boldsymbol{\Sigma}^{n+1})$ solutions of the implicit equation (16) we solve, as in [6], the associated fixed-point problem through Picard's iterations. Indeed, let us set $\boldsymbol{\Sigma}^{n,0} = \boldsymbol{\Sigma}^n$ and assume that, for $k \geq 0$, $\boldsymbol{\Sigma}^{n,k} \in \Lambda$ is known, we compute $\mathbf{u}^{n,k+1}$ by solving the linear diffusion equation

$$\begin{aligned} \rho^{n+1}\Big(\frac{\mathbf{u}^{n,k+1}-\mathbf{u}^n}{\delta t}\Big) - \mathrm{div}\Big(\frac{2\mu^{n+1}}{\mathfrak{Re}}\boldsymbol{D}\boldsymbol{u}^{n,k+1}\Big) + \rho^{n+1}\,\mathrm{div}(\mathbf{u}^n_{\mathrm{div}}\otimes\mathbf{u}^n) \\ +\boldsymbol{\nabla}(2p^n - p^{n-1}) \;=\; -\rho^{n+1}\mathbf{e_2} + \frac{\mathfrak{Bi}}{\mathfrak{Re}}\;\mathrm{div}(\alpha^{n+1}\boldsymbol{\Sigma}^{n,k}). \end{aligned} \tag{19}$$

This is followed by an explicit and pointwise (*a.e.* in Ω) Bingham projection providing the plastic part of the stress tensor $\boldsymbol{\Sigma}^{n,k+1}$, namely

$$\boldsymbol{\Sigma}^{n,k+1} = \mathbb{P}_\Lambda\big(\boldsymbol{\Sigma}^{n,k} + \ell\alpha^{n+1}\boldsymbol{D}\boldsymbol{u}^{n,k+1} + \theta(\boldsymbol{\Sigma}^n - \boldsymbol{\Sigma}^{n,k})\big). \tag{20}$$

By iterating over k through equations (19) and (20), the sequence $(\mathbf{u}^{n,k}, \boldsymbol{\Sigma}^{n,k})$ converges geometrically to the solution of (16). Indeed we have proved in [4], the following result :

Theorem 1 If $8\theta + r\mathfrak{Bi}\frac{\max(\alpha_1,\alpha_2)^2}{\min(\mu_1,\mu_2)} \leq 8$, then, for all $n \geq 0$ the sequence $(\mathbf{u}^{n,k}, \boldsymbol{\Sigma}^{n,k})_k$ tends to $(\mathbf{u}^{n+1}, \boldsymbol{\Sigma}^{n+1})$ when k tends to infinity. Moreover the convergence is geometric with common ratio $1-\theta$.

Note that in the case $\theta = 0$, the sequence $(\mathbf{u}^{n,k}, \boldsymbol{\Sigma}^{n,k})_k$ still tends to $(\mathbf{u}^{n+1}, \boldsymbol{\Sigma}^{n+1})$ (see [7]) but the convergence is known to be very slow (see [6]).

4 Numerical implementation

Let $\Omega = \big(-\frac{1}{2}, \frac{1}{2}\big) \times \big(-2, 2\big)$ the computational domain. We define a Cartesian uniform mesh (x_i, y_j) and we denote by $h = \frac{1}{n_x} = \frac{4}{n_y}$ the mesh size, where n_x and n_y are the number of mesh cells in each spatial direction. Together with the mesh points, we associate the midpoints

$$x_{i+\frac{1}{2}} = \frac{1}{2}(x_i + x_{i+1}) \quad \text{and} \quad y_{j+\frac{1}{2}} = \frac{1}{2}(y_j + y_{j+1}).$$

Let a computational cell $K_{ij} = (x_i, x_{i+1}) \times (y_j, y_{j+1})$. As in the classical MAC scheme for the incompressible Navier-Stokes equations (see [13]) the discrete velocity unknowns $\mathbf{u}_{ij} = (u_{ij}, v_{ij})$ are located at the midpoint of the cell edges, that is $u_{ij} \approx u(x_i, y_{j+1/2})$ and $v_{ij} \approx v(x_{i+1/2}, y_j)$. The discrete pressure p_{ij} and level set function ϕ_{ij} are placed at the center of the mesh cell K_{ij}, namely $p_{ij} \approx p(x_{i+1/2}, y_{j+1/2})$ and similarly for ϕ_{ij}. The components of the tensor $\boldsymbol{\Sigma}$ are also discretized at the center of the mesh cell. This choice is arbitrary but allows to update all tensor components, through the local projection (20), at the same mesh locations. Figure 1 summarizes the staggered arrangement of the unknowns. Centered second-order finite volume schemes are applied to discretize the spatial partial derivatives operator in Equations (15)-(18). The control volumes are: K_{ij} for the level set function (15) and the pressure increment (17), $K_{i,j+1/2} = (x_{i-1/2}, x_{i+1/2}) \times (y_j, y_{j+1})$ for the horizontal component of the velocity u_{ij} and $K_{i+1/2,j} = (x_i, x_{i+1}) \times (y_{j-1/2}, y_{j+1/2})$ for the

vertical component of the velocity v_{ij} which correspond to Equations (16) and (18). The Bingham projection (20) is enforced at points $(x_{i+1/2}, y_{j+1/2})$. Details on the discretization of the plastic contribution in the momentum equation and on the discrete contribution, with ghost points, of the boundary conditions are provided in [6].

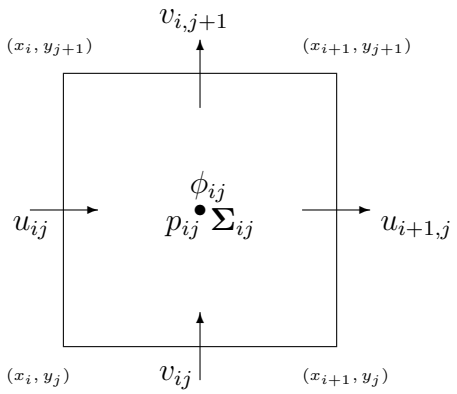

Figure 1: Location of the discrete unknowns in the mesh cell $K_{ij} = (x_i, x_{i+1}) \times (y_j, y_{j+1})$.

The level set equations (15) are discretized with a finite volume WENO scheme of order 5 (see [24, 15]). Even if it is initialized as the signed distance from the interface, the level set function computed with the fully discrete transport equation will not remain a distance function. As it is suggested in [26], a redistancing algorithm has to be applied periodically in time. That is, knowing ϕ^{n+1}, the following Hamilton-Jacobi equation is solved

$$\begin{cases} \frac{\partial \Phi}{\partial \tau} + \mathrm{sgn}(\phi^{n+1}) \Big(\|\boldsymbol{\nabla} \Phi\| - 1 \Big) = 0, \\ \Phi(\tau = 0) = \phi^{n+1}, \end{cases} \tag{21}$$

where τ is a fictitious time and

$$\mathrm{sgn}(\phi^{n+1}) = \begin{cases} -1 & \text{if} \quad \phi < 0, \\ 0 & \text{if} \quad \phi = 0, \\ 1 & \text{if} \quad \phi > 0. \end{cases}$$

Equation (21) is discretized as in [17] with a second-order TVD Runge-Kutta method as time marching scheme and second-order ENO finite-differences are applied for the spatial resolution. Stationary solutions Φ_s of (21) are distance functions, *i.e.* $\|\boldsymbol{\nabla} \Phi_\mathrm{s}\| = 1$, and share their interface $\{\mathbf{x} \in \Omega;\, \Phi_\mathrm{s}(\mathbf{x}) = 0\}$ with ϕ^{n+1}. This property is not preserve with a standard second-order ENO spatial discretization. Indeed, displacement of the interface has been observed during the fictitious time iterations of the reinitialization procedure. In [17], a subcell resolution near the interface modifying the ENO scheme has been proposed. The purpose of the subcell resolution is to fix the position of the interface, the zeros of the level set function ϕ^{n+1}, during the reinitialization iterations.

As in [22], the Heaviside function used to evaluate the density, the viscosity and the yield stress in terms of the level set function in (14) is replaced by the following regularized

Heaviside function

$$H_\epsilon(\phi) = \begin{cases} 0 & \text{if} \quad \phi < -\epsilon, \\ \frac{1}{2}\Big(1 + \frac{\phi}{\epsilon} - \frac{1}{\pi}\sin(\frac{\pi\phi}{\epsilon})\Big) & \text{if} \quad -\epsilon \leq \phi \leq \epsilon, \\ 1 & \text{if} \quad \phi > \epsilon. \end{cases}$$

Regularization of the viscosity coefficient across the interface is required in order to ensure the continuity of the viscous stress. Note that other regularization formulae could be used (see [27]). In the spatial discretization of the viscous terms present in the discrete momentum equation, the viscosity coefficient has to be evaluated both at the center of the mesh cells K_{ij} and at the mesh nodes (x_i, y_j). For the latter, second-order spatial interpolation is applied.

The implementation has been done in the F90/MPI code written for one phase Bingham flows [6]. The PETSc library [1, 2] is used to solve linear systems and to manage data on structured grids. The communications between the MPI processes are explicitly written with the help the MPI library.

5 Numerical results

In order to both estimate the convergence rate of the numerical scheme with respect to the temporal discretization and illustrate the performance of the method, we have performed simulations of the development of a Rayleigh-Taylor instability in the viscous regime. This problem consists of a heavy fluid lying above a lighter one in the rectangular domain $\Omega = (-1/2, 1/2) \times (-2, 2)$ under the action of a vertical downward gravitational field of intensity g. The density ratio is related to the Atwood number,

$$A_t = (\rho_2 - \rho_1)/(\rho_2 + \rho_1),$$

according to Tryggvason's definition [28] and the initial position of the interface is

$$y(x) = -0.1\cos(2\pi x).$$

In the rest of the paper, the density ratio is 3, so that $A_t = 0.5$, and $\mathfrak{Re} = 3000$. We assume that symmetry of the initial condition is maintained during the whole time evolution, so that the computational domain can be restricted to $(0, 1/2) \times (-2, 2)$. No-slip condition is enforced on the bottom and top walls and symmetry is imposed on the two vertical ones.

5.1 Time convergence

We first estimate the convergence rate of the numerical scheme with respect to the temporal discretization. We have performed numerical simulations with $\mathfrak{Bi} = 1$. The heavier fluid is a viscoplastic medium, that is to say $\alpha_2 = 1$, and the lighter one is Newtonian, *i.e.* $\alpha_1 = 0$. Values for r and θ are such that the hypothesis of Thereom 1 are satisfied and $\theta = \delta t$. With these parameters and starting from rest, a numerical simulation has

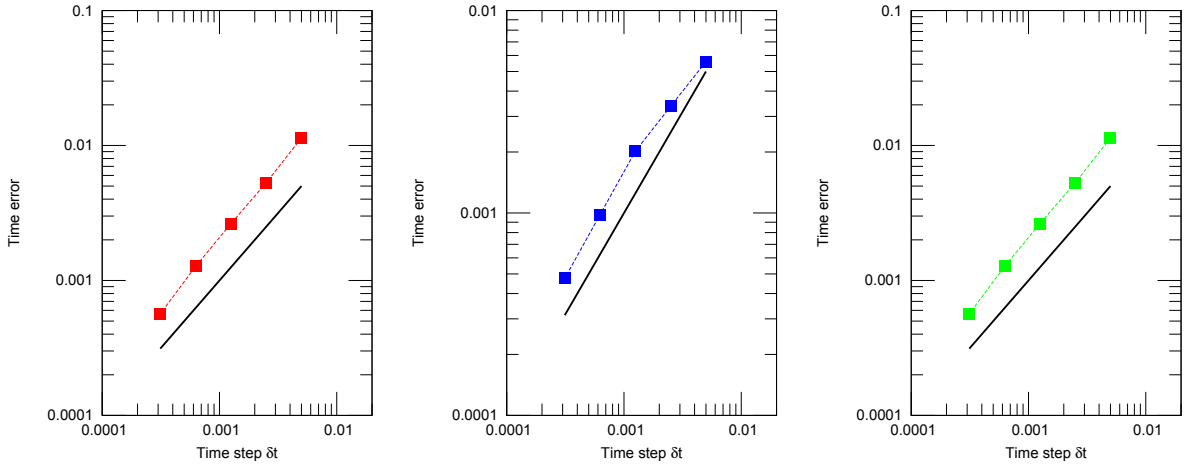

Figure 2: Error for the velocity, pressure and density in $L^2(\Omega)-$norm. The slope of the solid black line is 1 corresponding to an error in $\mathrm{O}(\delta t)$.

been performed up to the non-dimensional time $t = 1.8$ on a grid with 256×2048 mesh points and a time step $\delta t = 5 \times 10^{-5}$. Let us denote by $\mathbf{u}_{\mathrm{ref}}$, p_{ref} and ρ_{ref} the corresponding (discrete) velocity field, pressure and density. Note that the flow is not stationary at time $t = 1.8$. Indeed, the amplitude of the wave is of the order of $2.5d$.
In order to estimate the numerical error due to the time discretization, we have plotted on Figure 2 the L^2-norm of the difference between $\mathbf{u}_{\mathrm{ref}}$, p_{ref}, ρ_{ref} and $\mathbf{u}_{\delta t}$, $p_{\delta t}$, $\rho_{\delta t}$ computed on the same mesh with various increasing time steps $\delta t = 3.125 \times 10^{-4}$, $6.25 \times 10^{-4}, \ldots,$ 5×10^{-3}. In order to highlight the convergence rate, logarithmic scales are used. For this particular flow configuration, we recover the expected first order time accuracy for the bi-projection scheme proved in [4].

5.2 Numerical simulations of Rayleigh-Taylor instabilities

We first compute the development of a Rayleigh Taylor instability in the (test) case of Newtonian flows reported in [10], so that $\mathfrak{Bi} = 0$. Note that in our dimensionless model, we choose ρ_2 as reference density so that the Reynolds number is 3000 which corresponds to $\mathfrak{Re} = 1000$ in [10]. As in [10], finite differences are used for the time discretization but the front tracking method and the spatial discretization are different. The time evolution of the interface is shown in Figure 3 at times 1, 1.5, 1.75, 2, and 2.5 in the time scale of Tryggvason, which is related to ours by $t_{\mathrm{Tryg}} = t\sqrt{A_t}$. By comparing the positions of the falling and rising bubbles as the time evolves, a good agreement with the results in the pioneering work of [28] and the more recent ones in [10] is obtained. Differences are visible in the fine structures especially at the two last times but a similar behavior in the vortex structures can be observed. The numerical methods used to compute the interface are completely different: a level set formulation is used here while a stabilization with a nonlinear viscosity is added in the mass conservation equation in [10]. Therefore, we may not expect to obtain exactly the same (meaning with a pointwise comparison) fine turbulent like structures of the interface motion.

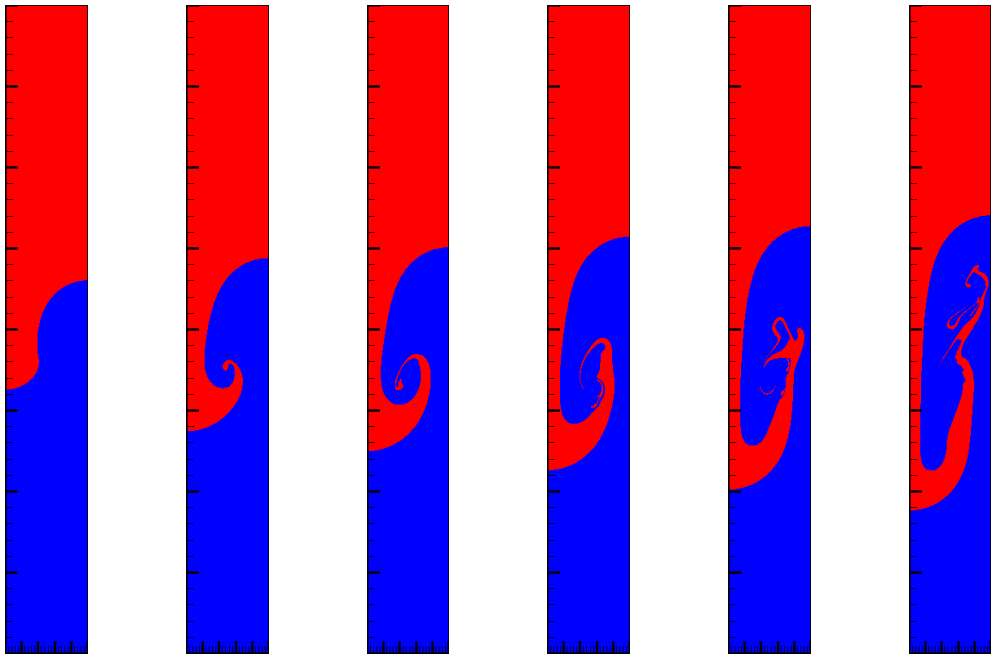

Figure 3: $\mathfrak{Re} = 3000$; $\mathfrak{Bi} = 0$, $\alpha_1 = \alpha_2 = 0$; density ratio 3. The interface is shown at times 1, 1.5, 1.75, 2, 2.25 and 2.5. The heavier fluid (ρ_2, α_2) corresponds to the red zone.

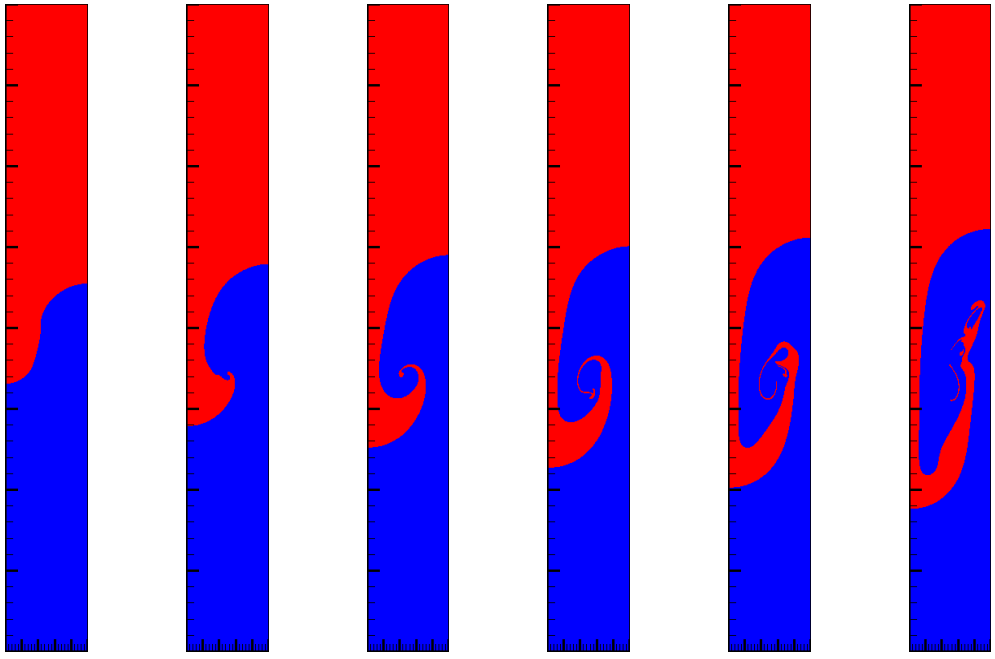

Figure 4: $\mathfrak{Re} = 3000$; $\mathfrak{Bi} = 10$, $\alpha_1 = 0$, $\alpha_2 = 1$; density ratio 3. The interface is shown at times 1, 1.5, 1.75, 2, 2.25 and 2.5. The heavier viscoplastic fluid (ρ_2, α_2) corresponds to the red zone.

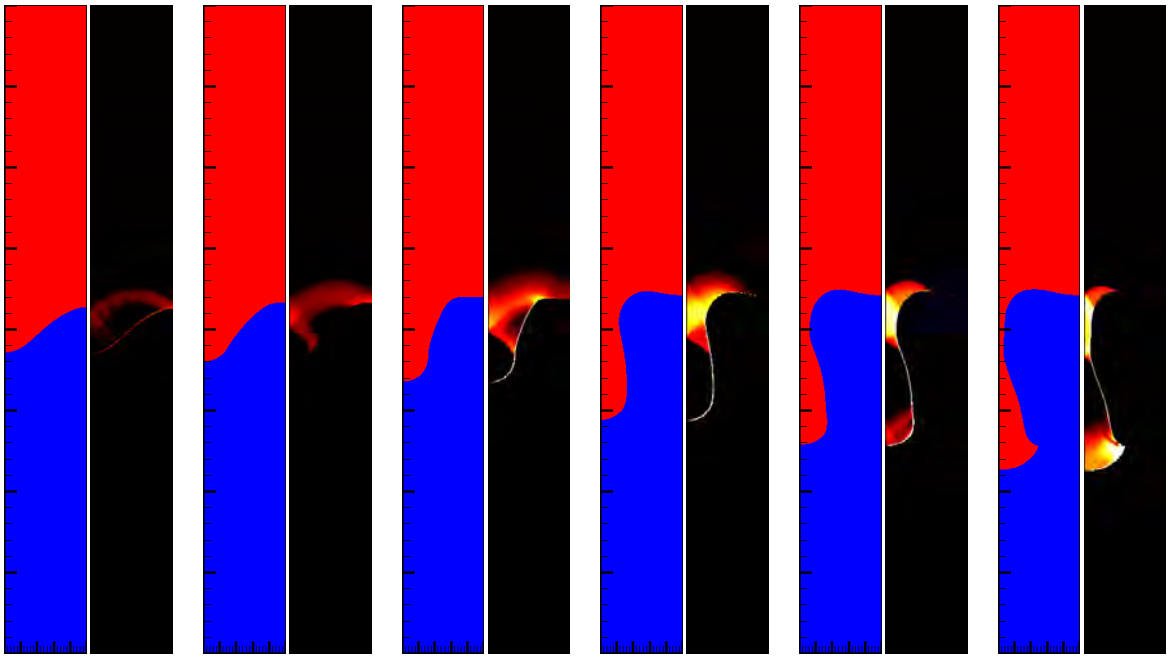

Figure 5: $\mathfrak{Re} = 3000$; $\mathfrak{Bi} = 75$, $\alpha_1 = 0$, $\alpha_2 = 1$; density ratio 3. Interface (left) and deformation rate $\|\boldsymbol{Du}\|$ in the viscoplastic phase (right) are shown at times 1, 1.5, 2, 2.5, 2.75 and 3. The heavier fluid (ρ_2, α_2) corresponds to the red zone.

We next compute a more challenging case, for the bi-projection scheme, where the heavier fluid is a Bingham medium ($\alpha_2 = 1$) while the lighter fluid is modeled with a Newtonian flow ($\alpha_1 = 0$). We first choose $\mathfrak{Bi} = 10$, and we report the time evolution of the interface at the same times as in the previous test case (see Figure 4). At this Bingham number, we first observe that the influence of this parameter on the positions of the falling and rising bubbles is not visible. Differences between Figures 3 and 4 appear in the shape of the falling structure in the early stage of the dynamics and also in the fine vortex structures developing during the fall of heavier viscoplastic medium. Note that at $t_{\text{Tryg}} = 1$, the head of the falling bubble has a different shape with an almost flat part.

We finally solve the same problem but for a much larger Bingham number $\mathfrak{Bi} = 75$. In order to highlight the impact of the Bingham number on the flow, at each time, we have simultaneously plotted on Figure 5 the position of the interface (on the left) and the deformation rate $\|\boldsymbol{Du}\|$ (on the right) in the viscoplastic phase. The values of $\|\boldsymbol{Du}\|$ shown are in the range $[10^{-15}, 10^{2}]$. There is almost no raising of the lighter fluid into the heavier one at this Bingham number. The heavier viscoplastic medium falls slowly and the shape of the falling bubble looks like a finger at times $2 \leq t_{\text{Tryg}} \leq 2.75$, *i.e.* a solid block almost rectangular sliding along the vertical symmetric axis. This is assessed by the rigid zone filling most of this finger. Unlike in the previous cases, there are no fine structures developing. The plastic zones (black regions on Figure 5) are located just behind the interface in the domain occupied by the viscoplastic medium at times $t_{\text{Tryg}} = 2$ and 2.5 while further in time, a deformation of the head of the falling bubble can be seen. Note, that at even larger Bingham number, we may expect that the heavier fluid will not flow.

6 Concluding remarks

We have proposed in this paper a first-order bi-projection scheme for the numerical simulation of two-phase immiscible, incompressible and isothermal flows of viscoplastic media. In order to track the interface between fluids a level set formulation is used. As in the Uzawa-like algorithm, the definition of the stress tensor is rewritten in terms of a pointwise projection and a pseudo-time relaxation term is added in order to achieve a geometric convergence of the fixed-point (Picard) iterations used for the computation of the plastic part of the stress tensor. A fractional time-stepping scheme is applied in order to handle the coupling between pressure and velocity field in the momentum equations. The interface between the two phases is tracked with a level set formulation and a redistancing algorithm is employed in order to ensure that the level set function remains a distance function, namely the normal signed distance from the interface. The spatial discretization is achieved with a second-order cell-centered finite volume schemes on a staggered mesh. The staggered location of the velocity unknowns allows to compute a free-divergence velocity field, up to the computer accuracy, which is used as transport velocity in the mass conservation equation. Numerical simulations of Rayleigh-Taylor instabilities are performed and presented. The first order rate of convergence with respect to the time step is recovered both in the case of Newtonian and Bingham flows. Comparisons with published results in the case of Newtonian flows validate the parallel implementation of the bi-projection scheme. Numerical simulations of a Bingham flow at $\mathfrak{Bi} = 10$ and 75 are reported and discussed. From the best of our knowledge, these results are the first ones obtained for this problem. At even larger Bingham number, we may expect that the heavier fluid will not flow. Investigating in more details the dynamics and behavior of Rayleigh-Taylor instabilities when the Bingham number is increased could be the scope of further works.

Acknowledgements This work is supported by the French Government Laboratory of Excellence initiative n°ANR-10-LABX-0006, by the French National Research Agency (ANR) RAVEX project, and by the French National Joint Research Program TelluS of INSU and INSMI CNRS (National Center for Scientific Research). This is Laboratory of Excellence ClerVolc contribution number 329.
The numerical simulations have been performed on a DELL cluster with 32 processors Xeon E2650v2 (8 cores), 1 To of total memory and an infiniband (FDR 56Gb/s) connecting network.

References

[1] S. Balay, S. Abhyankar, M.F. Adams, J. Brown, P. Brune, K. Buschelman, L. Dalcin, A. Dener, V. Eijkhout, W.D. Gropp, D. Kaushik, M.G. Knepley, Dave A. May, Lois Curfman McInnes, R. Tran Mills, T. Munson, K. Rupp, P. Sanan, B.F Smith, S. Zampini, H. Zhang, and H. Zhang. PETSc Web page. `http://www.mcs.anl.gov/petsc`, 2018.

[2] S. Balay, S. Abhyankar, M.F. Adams, J. Brown, P. Brune, K. Buschelman, L. Dalcin, A. Dener, V. Eijkhout, W.D. Gropp, D. Kaushik, M.G. Knepley, Dave A. May, Lois Curfman McInnes, R. Tran Mills, T. Munson, K. Rupp, P. Sanan, B.F Smith, S. Zampini, H. Zhang, and H. Zhang. PETSc users manual. Technical Report ANL-95/11 - Revision 3.10, Argonne National Laboratory, 2018.

[3] M. Bercovier and M. Engelman. A finite element method for incompressible non-Newtonian flows. *J. Comput. Phys.*, 36(3), 1980.

[4] R. Chalayer, L. Chupin, and T. Dubois. A bi-projection method for incompressible bingham flows with variable density, viscosity, and yield stress. *SIAM Journal on Numerical Analysis*, 56(4):2461–2483, 2018.

[5] Y.C. Chang, T.Y. Hou, B. Merriman, and S. Osher. A level set formulation of eulerian interface capturing methods for incompressible fluid flows. *J. Comput. Phys.*, 124, 1996.

[6] L. Chupin and T. Dubois. A bi-projection method for Bingham type flows. *Comput. Math. Appl.*, 72(5):1263–1286, 2016.

[7] J.D. Edward, R. Glowinski, and G. Guidoboni. On the numerical simulation of Bingham visco-plastic flow: Old and new results. *Journal of Non-Newtonian Fluid Mechanics*, 142(1–3):36 – 62, 2007. Viscoplastic fluids: From theory to application.

[8] I.A. Frigaard and C. Nouar. On the usage of viscosity regularisation methods for visco-plastic fluid flow computation. *J. Non-Newton. Fluid Mech.*, 127(1):1 – 26, 2005.

[9] S. Gottlieb and C.-W. Shu. Total variation diminishing Runge-Kutta schemes. *Math. Comp.*, 67(221):73–85, 1998.

[10] J.-L. Guermond and A.J. Salgado. A splitting method for incompressible flows with variable density based on a pressure Poisson equation. *J. Comput. Phys.*, 228(8):2834–2846, 2009.

[11] J.-L. Guermond and A.J. Salgado. Error analysis of a fractional time-stepping technique for incompressible flows with variable density. *SIAM J. Numer. Anal.*, 49(3):917–944, 2011.

[12] J.L. Guermond, P. Minev, and J. Shen. An overview of projection methods for incompressible flows. *Comput. Methods Appl. Mech. Engrg.*, 195(44-47):6011–6045, 2006.

[13] F.H. Harlow and J.E. Welch. Numerical calculation of time-dependent viscous incompressible flow of fluid with free surface. *Phys. Fluids*, 12(8).

[14] Ioan R. Ionescu, Anne Mangeney, François Bouchut, and Olivier Roche. Viscoplastic modeling of granular column collapse with pressure-dependent rheology. *Journal of Non-Newtonian Fluid Mechanics*, 219:1 – 18, 2015.

[15] G.S. Jiang and D. Peng. Weighted eno schemes for hamilton-jacobi equations. *SIAM J. Sci. Comput*, 21(6):2126–2143, 2000.

[16] S. C. Loughlin, E. S. Calder, A. Clarke, P. D. Cole, R. Luckett, M. T. Mangan, D. M. Pyle, R. S. J. Sparks, B. Voight, and R. B. Watts. Pyroclastic flows and surges generated by the 25 june 1997 dome collapse, soufrière hills volcano, montserrat. *Geological Society, London, Memoirs*, 21(1):191–209, 2002.

[17] C. Min. On reinitializing level set functions. *J. Comput. Phys.*, 229, 2010.

[18] S. Osher and R. Fedkiw. *Level Set Methods and Dynamic Implicit Surfaces*, volume 153 of *Applied Mathematical Sciences*. Springer-Verlag, New-York, 2003.

[19] S. Osher and R.P. Fedkiw. Level set methods: An overview and some recent results. *J. Comput. Phys.*, 169(2):463–502, 2001.

[20] T.C. Papanastasiou. Flows of materials with yield. *J. Rheol.*, 31(5):385–404, 1987.

[21] R. Paris. Source mechanics of volcanic tsunamis. *Phil. Trans. R. Soc. A*, 373:20140380, 2015.

[22] G. Russo and P. Smereka. A remark on computing distance functions. *J. Comput. Phys.*, 163, 2000.

[23] P. Saramito and A. Wachs. Progress in numerical simulation of yield stress fluid flows. *Rheologica Acta*, 56(3):211–230, 2017.

[24] C.-W. Shu and S. Osher. Efficient implementation of essentially non-oscillatory shock-capturing schemes. *J. Comput. Phys.*, 77(2):439–471, 1988.

[25] M. Sussman, E. Fatemi, P. Smereka, and S. Osher. An improved level set method for incompressible two-phase flows. *Comp. Fluids*, 27(5-6), 1998.

[26] M. Sussman, P. Smereka, and S. Osher. A level set approach for computing solutions to incompressible two-phase flow. *J. Comput. Phys.*, 114, 1994.

[27] M. Sussman, K.M. Smith, M.Y. Hussaini, M. Otha, and R. Zhi-Wei. A sharp interface method for incompressible two-phase flows. *J. Comput. Phys.*, 221(2).

[28] G. Tryggvason. Numerical simulations of the rayleigh-taylor instability. *J. Comput. Phys.*, 75(2):253–282, April 1988.

[29] P. Watts and C. F. Waythomas. Theoretical analysis of tsunami generation by pyroclastic flows. *Journal of Geophysical Research: Solid Earth*, 108(B12).